ACS APPLIED MATERIALS & INTERFACES

Research Article

www.acsami.org

Comparison of the Electrochemical Performance of $NiMoO_4$ Nanorods and Hierarchical Nanospheres for Supercapacitor Applications

Daoping Cai, Dandan Wang, Bin Liu, Yanrong Wang, Yuan Liu, Lingling Wang, Han Li, Hui Huang, Qiuhong Li, and Taihong Wang*

Pen-Tung Sah Institute of Micro-Nano Science and Technology, Xiamen University, Xiamen 361000, China

Supporting Information

ABSTRACT: Much attention has been paid to exploring electrode materials with enhanced supercapacitor performance as well as relatively low cost and environmental friendliness. In this work, $NiMoO_4$ nanospheres and nanorods were synthesized by facile hydrothermal methods. The hierarchical $NiMoO_4$ nanospheres were about 2.5 μm in diameter and assembled from thin mesoporous nanosheets with a thickness of about 10−20 nm. The $NiMoO_4$ nanorods were about 80 nm in diameter and about 300 nm to 1 μm in length. Their electrochemical properties were investigated for use as electrode materials for supercapacitors (SCs). The $NiMoO_4$ nanospheres exhibited a higher specific capacitance and better cycling stability and rate capability, which were attributed to their large surface area and high electrical conductivity. The specific capacitances were 974.4, 920.8, 875.5, 859.1, and 821.4 F/g at current densities of 1, 2, 4, 6, and 10 A/g, respectively. Remarkably, the energy density was able to reach 20.1 Wh/kg at a power density of 2100 W/kg. After 2000 cycles, the $NiMoO_4$ nanospheres still displayed a high specific capacitance of about 631.8 F/g at a current density of 5 A/g. These results implied that the hierarchical $NiMoO_4$ nanospheres could be a promising candidate for use as high-performance SCs.

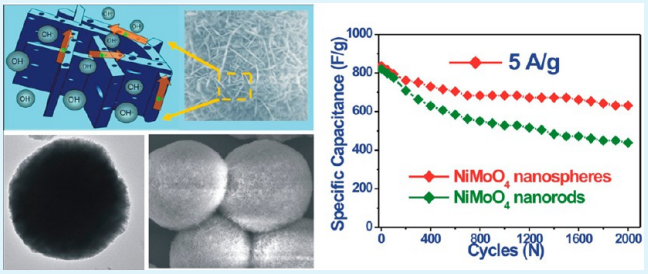

KEYWORDS: *nickel molybdate, hydrothermal method, mesoporous, electrode material, supercapacitors*

1. INTRODUCTION

The energy-storage problem is one of the great challenges in the twenty-first century. The investigation of high-performance, low-cost, and environmentally friendly energy-storage systems has been faced an ever increasing demand because of the urgent needs of modern society.[1] Supercapacitors (SCs), also called electrochemical capacitors (ECs), have attracted more and more attention and are considered to be one of the most promising candidates for use as energy sources among various emerging energy-storage technologies because of their high power density, fast charge/discharge process, environmental friendliness, and long lifespan.[2,3] In general, according to their charge-storage mechanisms, SCs can be classified into two kinds: electrical double-layer capacitors (EDLCs) and Faradaic pseudocapacitors.[4] In electrical double-layer capacitors (EDLCs), charge is accumulated at the interface between the electrode materials and the electrolyte solution (such as carbon-based materials);[5,6] Faradaic pseudocapacitors store energy by fast and reversible redox reactions between electrolyte and electrode materials on the electrode surface (such as metal oxides/hydroxides and conducting polymers).[6−9] In contrast to the electrical double-layer capacitors (EDLCs), Faradaic pseudocapacitors can achieve much higher specific capacitance and energy density because of their reversible redox reactions.[9−11]

Although scientists have made a lot of progress in electrode materials for SCs, these electrode materials are still limited by low capacitance (e.g., carbon-based materials),[12,13] high cost (e.g., RuO_2-based materials),[14,15] or harm to the environment (e.g., metal sulfide),[16] which has seriously hindered the development of SCs. Among metal oxides, binary metal oxides are considered to be potential materials for high-performance SCs because of their feasible oxidation state and high electrical conductivity.[17] Recently, metal molybdates, such as $CoMoO_4$, $NiMoO_4$, and $MnMoO_4$, have been extensively studied.[18−20] Among them, $NiMoO_4$ possesses a higher specific capacitance because of the high electrochemical activity of the nickel ion.[18] However, the complex nature of molybdates makes the synthesis of nanostructured $NiMoO_4$ difficult. Until now, there have been only a few reports on using $NiMoO_4$ as an electrode material for supercapacitor applications. Therefore, it is of great significance to develop a simple method to synthesize nanostructured $NiMoO_4$ with unique morphologies and enhanced capacitive behavior.

In this work, we report for the first time a simple one-pot hydrothermal method to synthesize hierarchical $NiMoO_4$

Received: August 16, 2013
Accepted: November 26, 2013
Published: November 26, 2013

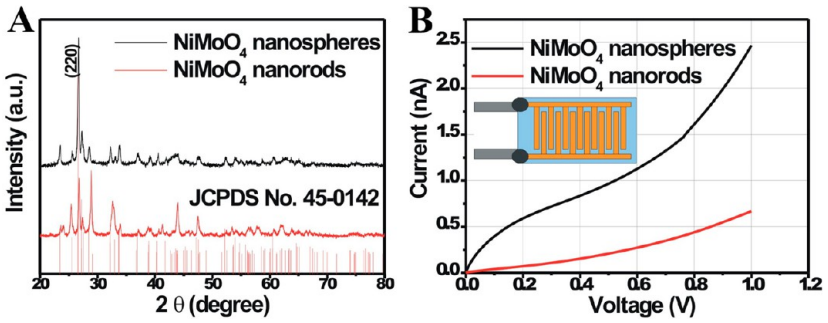

Figure 1. (A) XRD patterns and (B) $I-V$ curves of the as-prepared $NiMoO_4$ nanospheres and nanorods (inset shows the schematic of the Au interdigital electrode).

nanospheres assembled from thin mesoporous nanosheets and investigated their electrochemical performance as electrode material for SCs. For comparison, $NiMoO_4$ nanorods were also synthesized and investigated for use as electrode material for SCs. The unique hierarchical $NiMoO_4$ nanospheres showed higher specific capacitance and better cycling stability and rate capability. It is believed that the hierarchical $NiMoO_4$ nanospheres could serve as a promising candidate for supercapacitor materials because of tirhe high capacity and low cost as well as environmental friendliness.

2. EXPERIMENTAL DETAILS

2.1. Material Synthesis. In a typical synthesis of the hierarchical $NiMoO_4$ nanospheres, 1 mmol of $Na_2MoO_4{\cdot}7H_2O$ and 1 mmol of $Ni(CH_3COO)_2{\cdot}4H_2O$ were added into 30 mL of distilled water. The mixture was kept under an intense ultrasonic treatment for a few minutes to form a uniform solution. The resulting solution was transferred to a Teflon-lined stainless steel autoclave and kept at 140 °C for 12 h. The products were collected by centrifugation at 8000 rpm and washed several times with distilled water and ethanol. Finally, the as-prepared hydrate precursor was annealed at 500 °C for 4 h in air with a heating rate of 2 °C/min to obtain the hierarchical $NiMoO_4$ nanospheres.

In a typical synthesis of the $NiMoO_4$ nanorods, 1 mmol of $Na_2MoO_4{\cdot}7H_2O$ and 1 mmol of $Ni(NO_3)_2{\cdot}6H_2O$ were added into 30 mL of ethanol/distilled water (1:1 v/v). The mixture was kept under an intense ultrasonic treatment for a few minutes to form a uniform solution. The resulting solution was transferred to a Teflon-lined stainless steel autoclave and kept at 140 °C for 12 h. The products were collected by centrifugation at 8000 rpm and washed several times with distilled water and ethanol. Finally, the as-prepared hydrate precursor was annealed at 500 °C for 4 h in air with a heating rate of 2 °C/min to obtain the $NiMoO_4$ nanorods.

2.2. Material Characterization. The composition and phase of the as-prepared products were determined by the powder XRD pattern, recorded on a Panalytical X-pert diffractometer with Cu Kα radiation. The morphology and crystal structure of the as-prepared products were observed by scanning electron microscopy (SEM, Hitachi S4800) and high-resolution transmission electron microscopy (HRTEM JEM 2100) with an acceleration voltage of 200 kV. The TEM sample was prepared by depositing a drop of diluted suspension in ethanol on a copper grid coated with carbon film. The $I-V$ curves were obtained by an Agilent 4156C precision semiconductor parameters analyzer with a JANIS ST-500 probe station. The device was fabricated by a simple drop-casting method. The as-prepared $NiMoO_4$ was suspended in ethanol by intense sonication, and then a small drop (2.5 μl) of the suspension was dropped on the Au interdigital electrodes. N_2 adsorption−desorption was determined by Brunauer−Emmett−Teller (BET) measurements using a Tristar-3000 surface-area analyzer.

2.3. Electrochemical Measurements. The electrochemical measurements were carried out in a three-electrode electrochemical cell containing a 3 M KOH aqueous solution as the electrolyte. The working electrode was fabricated by mixing 80 wt % of electrode material, 10 wt % of carbon black, and 10 wt % of poly(vinylidene difluoride) (PVDF, Aldrich) using *N*-methyl-2-pyrrolidone as the solvent to yield a slurry. Then, the slurry was pressed onto the nickel foam current collector and dried at 80 °C in a vacuum oven for 12 h. The mass of electrode material was about 3.0 mg in each working electrode. The electrochemical measurements were carried out on a CHI660E electrochemical workstation. A standard calomel electrode (SCE) was used as the reference electrode and a Pt foil, as the counter electrode, and all of the experiments were done at ambient temperature. The specific capacitance (C), energy density (E), and power density (P) were calculated according to the following equations[21,22]

$$C = \frac{\int IdV}{\upsilon m V} \quad (1)$$

$$C = \frac{It}{mV} \quad (2)$$

$$E = \frac{1}{2}CV^2 \quad (3)$$

$$P = \frac{E}{t} \quad (4)$$

where I is the constant discharge current (A), υ is the potential scan rate (mV/s), t is the discharge time (s), V is the potential window (V), and m is the mass (g) of the active material on the electrode.

3. RESULTS AND DISCUSSION

3.1. Synthesis and Characterization of the $NiMoO_4$ Nanospheres and Nanorods. At first, the as-synthesized products were characterized by powder XRD analysis. Figure 1A shows the typical powder X-ray diffraction (XRD) patterns of the as-prepared products. The characteristic (220) peak at 26.6° is the typical peak of β-$NiMoO_4$, indicating the successful formation of β-$NiMoO_4$.[23] The XRD pattern of the $NiMoO_4$ nanospheres could be indexed to the monoclinic structured $NiMoO_4$ with a space group of $C2/m$ (JCPDS card no. 45-0142). However, for the $NiMoO_4$ nanorods, the peaks around 28°, 33°, and 44° were quite different, which were attributed to α-$NiMoO_4$ (JCPDS card no. 33-0948).[23−25] The β-$NiMoO_4$ phase was not stable at room temperature, and upon cooling to room temperature, some β-$NiMoO_4$ transformed into α-$NiMoO_4$. Importantly, it has been noted that the electrical conductivity of the β-$NiMoO_4$ is much higher than α-$NiMoO_4$.[25] Therefore, the $NiMoO_4$ nanospheres were expected to possess a higher electrical conductivity than the $NiMoO_4$ nanorods. It is well-accepted that electrode materials with high electrical conductivity possess an enhanced electrochemical

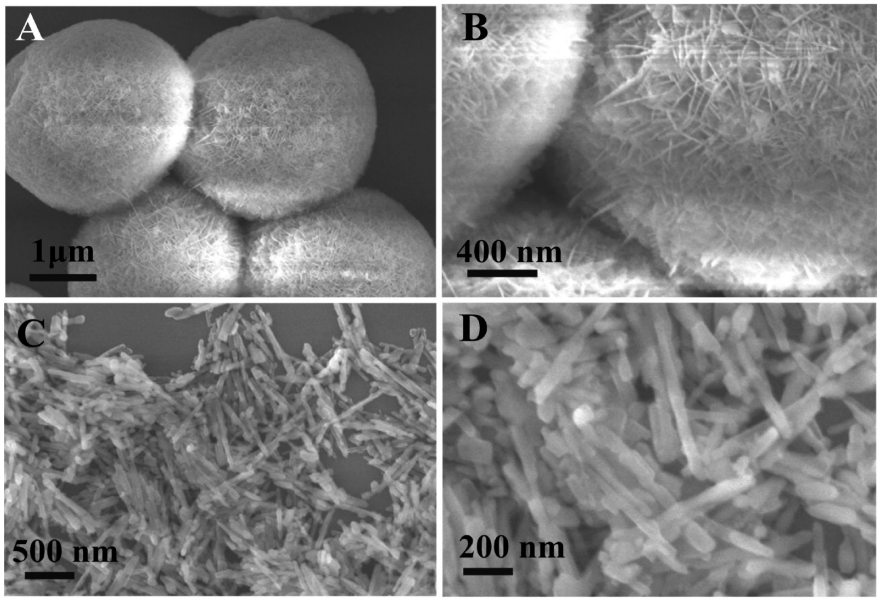

Figure 2. Typical SEM images of the $NiMoO_4$ nanospheres at (A) low magnification and (B) high magnification and typical SEM images of the $NiMoO_4$ nanorods at (C) low magnification and (D) high magnification.

performance for SCs because of the fast electron transport.[26] The electrical conductivity of the $NiMoO_4$ nanospheres and nanorods were investigated using a precision semiconductor parameters analyzer with a JANIS ST-500 probe station. Figure 1B shows the $I-V$ curves of the as-prepared $NiMoO_4$ nanospheres and nanorods. As is evident from the curves, the $NiMoO_4$ nanospheres exhibited a higher electrical conductivity than the $NiMoO_4$ nanorods, which was in good agreement with the above hypothesis.

The morphologies of the products were detected by SEM. Figure 2A,B shows the representative scanning electron microscopy (SEM) images of the as-prepared products. Hierarchical $NiMoO_4$ nanospheres with an average diameter of 2.5 μm were observed from the SEM images. The magnified image shows that the hierarchical spheres were assembled from thin nanosheets. These nanosheets with a thickness of about 10−20 nm were connected to each other to form a stable hierarchical structure. Figure 2C,D shows the SEM images of the $NiMoO_4$ nanorods. The diameter of the nanorods was about 80 nm, and the length of the nanorods was in the range from 300 nm to 1 μm.

The as-prepared products were further characterized by TEM. As shown in Figure 3A, the nanosphere structure was also demonstrated from TEM observation, which was consistent with the SEM observation. Interestingly, the magnified view of the nanosheets (Figure 3B) indicated the mesoporous feature of the thin nanosheets. The formation of mesopores is generally attributed to the release of water molecules during the thermal treatment.[27] The high-resolution transmission electron microscopy (HRTEM) image taken from an individual nanosheet is shown in Figure 3C. The lattice fringes showed an interplanar spacing of 0.24 nm, corresponding to the (400) crystal planes. The SAED pattern (inset in Figure 3C) further confirmed the polycrystalline nature of the thin nanosheets. Figure 3D,E shows the TEM images of the $NiMoO_4$ nanorods at different magnifications. The high-resolution transmission electron microscopy (HRTEM) image is shown in Figure 3F. The lattice fringes showed an interplanar spacing of 0.27 nm, corresponding to the (112) crystal planes.

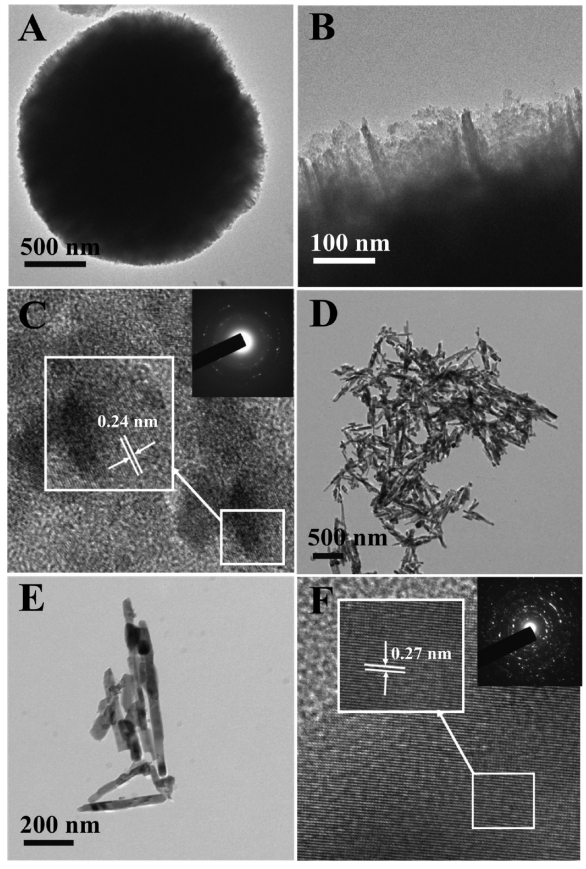

Figure 3. TEM images of an individual $NiMoO_4$ nanosphere at (A) low magnification and (B) high magnification and (C) HRTEM image with the inset showing the corresponding SAED pattern. TEM images of the $NiMoO_4$ nanorods at (D) low magnification and (E) high magnification and (F) HRTEM image with the inset showing the corresponding SAED pattern.

The SAED pattern (inset in Figure 3F) indicated its polycrystalline characteristics. The compositions of the

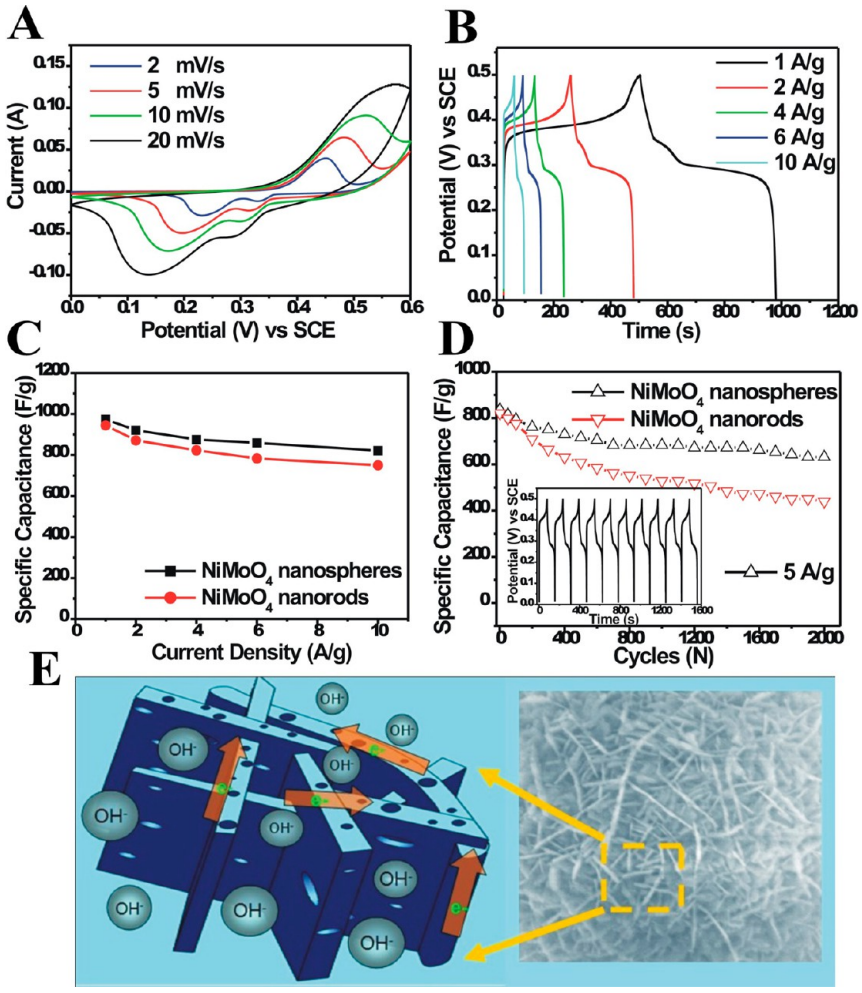

Figure 4. Electrochemical characterizations of the $NiMoO_4$ nanospheres and nanorods in a 3 M KOH aqueous solution. (A) Cyclic voltammetry (CV) curves and (B) galvanostatic charge−discharge curves of the $NiMoO_4$ nanospheres. (C) Capacitance as a function of current density. (D) Capacitance cycling performance at a constant current density of 5 A/g (inset shows the first 10 galvanostatic charge−discharge voltage profiles of the $NiMoO_4$ nanospheres at a current density of 5 A/g). (E) Schematic illustration of the basis for the excellent electrochemical performance of the $NiMoO_4$ nanospheres.

$NiMoO_4$ nanospheres and nanorods were also determined by energy-dispersive X-ray spectroscopy (EDS) analysis under a N_2 atmosphere. As shown in Figure S1, the Ni, Mo, and O peaks were observed in this spectrum, suggesting that the samples were composed of mainly Ni, Mo, and O. The signal of Cu was from the copper grid. Moreover, mapping results indicated that Ni, Mo, and O were homogeneously and uniformly distributed throughout the samples (Figure S2). Meanwhile, the nitrogen adsorption−desorption experiments revealed that the surface area of the $NiMoO_4$ nanospheres (58.2 m^2/g) was much higher than the $NiMoO_4$ nanorods (13.5 m^2/g), as shown in Figure S3. The BJH pore-size distribution provided information about the mesoporosity of the $NiMoO_4$ nanospheres, which was consistent with the TEM result (inset in Figure S3). The high BET surface area and mesoporous structure of the $NiMoO_4$ nanospheres provided the possibility of the efficient transport of electrons and ions, leading to the high electrochemical capacity of the electrode material.[8]

3.2. Electrochemical Investigation. It is widely accepted that the electrochemical properties of the electrode materials are largely related to their morphologies and sizes.[8,28−30] The electrochemical measurements of the $NiMoO_4$ nanospheres and nanorods as electrode materials for SCs were carried out in a three-electrode electrochemical cell containing a 3 M KOH aqueous solution as the electrolyte. At first, cyclic voltammetry (CV) was tested within the potential range of 0−0.60 V (vs SCE) at various scan rates. Typical CV curves of the $NiMoO_4$ nanospheres under various scan rates are shown in Figure 4A. Each CV curve consisted of strong redox peaks, which confirmed that the capacitance characteristics were governed by Faradaic reactions.[17,21] According to eq 1, a high specific capacitance of 1048.8 F/g was obtained at a scan rate of 2 mV/s. With increasing scan rates, the potential of the oxidation peak shifted in the positive direction and that of the reduction peak shifted in the negative direction, which was related mainly to the internal resistance of the electrode.[22] Figure 4B shows the galvanostatic charge−discharge profiles of the $NiMoO_4$ nanospheres at different current densities ranging from 1 to 10 A/g. It was observed that there were voltage plateaus around 0.30 V, which is consistent with the CV curves. On the basis of eq 2, the specific capacitances of the $NiMoO_4$ nanospheres were calculated to be 974.4, 920.8, 875.5, 859.1, and 821.4 F/g at current densities of 1, 2, 4, 6, and 10 A/g, respectively. The specific capacitances of the $NiMoO_4$ nanorods were calculated to be 944.8, 871.2, 823.1, 783.5, and 750.0 F/g at current

densities of 1, 2, 4, 6, and 10 A/g, respectively. These results implied that the $NiMoO_4$ nanospheres exhibited a higher capacitance and better rate capability. The capacitance as a function of current density is plotted in Figure 4C. It is worth noting that the capacitances are much higher than the other reported electrode materials including carbon-based materials,[5] RuO_2,[15] Co_3O_4,[29] MnO_2,[10] NiO,[31] and so forth. The power density (P) and energy density (E) can be further calculated from the galvanostatic discharge curves based on eqs 3 and 4. For the $NiMoO_4$ nanospheres, the energy densities were 32.2, 29.5, 26.4, 23.8, and 20.1 Wh/kg, and the power densities were 244, 480, 932, 1341, and 2100 W/kg at current densities of 1, 2, 4, 6, and 10 A/g, respectively. For the $NiMoO_4$ nanorods, the energy densities were 31.6, 28.2, 24.9, 23.1, and 20.2 Wh/kg, and the power densities were 245.5, 483, 934, 1383, and 2200 W/kg at current densities of 1, 2, 4, 6, and 10 A/g, respectively. It is worth mentioning that both the $NiMoO_4$ nanospheres and nanorods showed high power density and energy density, which were comparable to literatures results.[32,33]

In addition, the long-term cycle stability of the $NiMoO_4$ nanospheres and nanorods was also investigated by repeating the chronopotentiometry (CP) tests at a current density of 5 A/g for 2000 cycles. As shown in Figure 4D, after 2000 cycles, the $NiMoO_4$ nanospheres still displayed a high specific capacitance of about 631.8 F/g at a current density of 5 A/g (about 25.5% specific capacitance loss). However, the $NiMoO_4$ nanorods displayed a high specific capacitance of about 438.5 F/g at a current density of 5 A/g (about 47.6% specific capacitance loss). These results revealed the better cycling stability of the $NiMoO_4$ nanospheres. The cycling behavior was similar to $CoMoO_4$−$NiMoO_4{\cdot}nH_2O$ bundle electrode. The capacitance loss occurred mainly during the first several hundred cycles and then remained stable after this stage.[18] The decay of the capacitance is generally explained by the mechanical expansion of the electrode material during the ion-insertion/removal process and the dissolution of some electrode material during the cycling.[34] EIS measurements were performed by applying an ac voltage with 5 mV amplitude in a frequency range from 0.01 Hz to 100 kHz. As shown in Figure S4, both the $NiMoO_4$ nanospheres and nanorods exhibited small semicircles in the impedance plots, indicating small charge-transfer resistance (R_{ct}). The internal resistance (R_e) values of the $NiMoO_4$ nanospheres and nanorods were 0.61 and 0.98 Ω, indicating the improved electrical conductivity of the $NiMoO_4$ nanospheres,[18,35] which was consistent with the I−V results. These results demonstrate the high specific capacitance and excellent cycling property of the hierarchical $NiMoO_4$ nanospheres, making them a promising electrode material for practical applications. Compared with the $NiMoO_4$ nanorods, the superior electrochemical performance of the $NiMoO_4$ nanospheres is mainly attributed to their large surface area and high electrical conductivity. The $NiMoO_4$ nanospheres were assembled by thin mesoporous nanosheets (Figure 4E). These interconnected nanosheets with high conductivity are advantageous for fast electron transport.[26] The thin and mesoporous nanostructure could provide efficient ion and electron transport, giving rise to faster kinetics and resulting in high charge/discharge capacities even at high current densities.[36,37] Moreover, the thin and mesoporous characteristics of the nanosheets resulted in large surface area, providing more electroactive sites for Faradaic energy storage.[38,39]

4. CONCLUSIONS

We have successfully synthesized $NiMoO_4$ nanospheres and nanorods through simple hydrothermal methods, and their electrochemical properties were investigated. Compared with the $NiMoO_4$ nanorods, the $NiMoO_4$ nanospheres were almost in the form of β-$NiMoO_4$ but with a higher electrical conductivity. Moreover, the $NiMoO_4$ nanospheres were assembled from many thin mesoporous nanosheets, resulting in a larger surface area. Taking advantage of these unique structural features, the $NiMoO_4$ nanospheres showed enhanced electrochemical performance compared with the $NiMoO_4$ nanorods. Our results indicate that the hierarchical $NiMoO_4$ nanospheres hold great promise for use as an advanced electrode material for high-performance SCs. It is believed that this study can contribute to the rational design and synthesis of electrode materials for advanced supercapacitor applications.

■ ASSOCIATED CONTENT

Supporting Information

EDS, BET, and EIS characterization of the $NiMoO_4$ nanospheres and nanorods. This material is available free of charge via the Internet at http://pubs.acs.org.

■ AUTHOR INFORMATION

Corresponding Author

*Tel.:+86-0592-2187196; Fax: +86-0592-2197196; E-mail: thwang@xmu.edu.cn.

Notes

The authors declare no competing financial interest.

■ ACKNOWLEDGMENTS

This research was partly supported by the National Basic Research Program of China (grant no. 2007CB310500) and the National Natural Science Foundation of China (grant no. 61376073).

■ REFERENCES

(1) Arico, A. S.; Bruce, P.; Scrosati, B.; Tarascon, J. M.; Schalkwijk, W. V. *Nat. Mater.* **2005**, *4*, 366−377.
(2) Simon, P.; Gogotsi, Y. *Nat. Mater.* **2008**, *7*, 845−854.
(3) Wang, G. P.; Zhang, L.; Zhang, J. J. *Chem. Soc. Rev.* **2012**, *41*, 797−828.
(4) Choi, D.; Blomgren, G. E.; Kumta, P. N. *Adv. Mater.* **2006**, *18*, 1178−1182.
(5) Zhang, L. L.; Zhao, X. S. *Chem. Soc. Rev.* **2009**, *38*, 2520−2531.
(6) Snook, G. A.; Kao, P.; Best, A. S. *J. Power Sources* **2011**, *196*, 1−12.
(7) Deng, W. T.; Ji, X. B.; Chen, Q. Y.; Banks, C. E. *RSC Adv.* **2011**, *1*, 1171−1178.
(8) Jiang, H.; Zhao, T.; Li, C. Z.; Ma, J. *J. Mater. Chem.* **2011**, *21*, 3818−3823.
(9) Huang, Y.; Liang, J. J.; Chen, Y. S. *Small* **2012**, *8*, 1805−1834.
(10) Yu, G. H.; Hu, L. B.; Vosgueritchian, M.; Wang, H. L.; Xie, X.; McDonough, J. R.; Cui, X.; Cui, Y.; Bao, Z. N. *Nano Lett.* **2011**, *11*, 2905−2911.
(11) Zhi, M. J.; Manivannan, A.; Meng, F. K.; Wu, N. Q. *J. Power Sources* **2012**, *208*, 345−353.
(12) Cheng, Y. W.; Lu, S. T.; Zhao, H. B.; Varanasi, C. V.; Liu, J. *Nano Lett.* **2012**, *12*, 4206−4211.
(13) Hsieh, C. T.; Hsu, S. M.; Lin, J. Y.; Teng, H. *J. Phys. Chem. C* **2011**, *115*, 12367−12374.
(14) Hu, C. C.; Chang, K. H.; Lin, M. C.; Wu, Y. T. *Nano Lett.* **2006**, *6*, 2690−2695.

(15) Zhang, J. T.; Ma, J. Z.; Zhang, L. L.; Guo, P. Z.; Jiang, J. W.; Zhao, X. S. *J. Phys. Chem. C* **2010**, *114*, 13608−13613.
(16) Wang, Q. H.; Jiao, L. F.; Du, H. M.; Peng, W. X.; Han, Y.; Song, D. W.; Si, Y. C.; Wang, Y. J.; Yuan, H. T. *J. Mater. Chem.* **2011**, *21*, 327−329.
(17) Zhang, G. Q.; Lou, X. W. *Adv. Mater.* **2013**, *25*, 976−979.
(18) Liu, M. C.; Kong, L. B.; Lu, C.; Ma, X. J.; Li, X. M.; Luo, Y. C.; Kang, L. *J. Mater. Chem. A* **2013**, *1*, 1380−1387.
(19) Liu, M. C.; Kang, L.; Kong, L. B.; Lu, C.; Ma, X. J.; Li, X. M.; Luo, Y. C. *RSC Adv.* **2013**, *3*, 6472−6478.
(20) Mai, L. Q.; Yang, F.; Zhao, Y. L.; Xu, X.; Xu, L.; Luo, Y. Z. *Nat. Commun.* **2011**, *2*, 381−385.
(21) Qu, B. H.; Chen, Y. J.; Zhang, M.; Hu, L. L.; Lei, D. N.; Lu, B. G.; Li, Q. H.; Wang, Y. G.; Chen, L. B.; Wang, T. H. *Nanoscale* **2012**, *4*, 7810−7816.
(22) Yan, J.; Fan, Z. J.; Sun, W.; Ning, G. Q.; Wei, T.; Zhang, Q.; Zhang, R. F.; Zhi, L. J.; Wei, F. *Adv. Funct. Mater.* **2012**, *22*, 2632−2641.
(23) Xiao, W.; Chen, J. S.; Li, C. M.; Xu, R.; Lou, X. W. *Chem. Mater.* **2010**, *22*, 746−754.
(24) Rodriguez, J. A.; Chaturvedi, S.; Hanson, J. C. *J. Phys. Chem. B* **1998**, *102*, 1347−1355.
(25) Moreno, B.; Chinarro, E.; Colomer, M. T.; Jurado, J. R. *J. Phys. Chem. C* **2010**, *114*, 4251−4257.
(26) Chen, H.; Jiang, J.; Zhang, L.; Wan, H.; Qi, T.; Xia, D. *Nanoscale* **2013**, *5*, 8879−8883.
(27) Li, J. T.; Zhao, W.; Huang, F. Q.; Manivannan, A.; Wu, N. Q. *Nanoscale* **2011**, *3*, 5103−5109.
(28) Chen, J. S.; Ng, M. F.; Wu, H. B.; Zhang, L.; Lou, X. W. *CrystEngComm* **2012**, *14*, 5133−5136.
(29) Meher, S. K.; Rao, G. R. *J. Phys. Chem. C* **2011**, *115*, 15646−15654.
(30) Wang, J.; Polleux, J.; Lim, J.; Dunn, B. *J. Phys. Chem. C* **2007**, *111*, 14925−14931.
(31) Han, D. D.; Xu, P. C.; Jing, X. Y.; Wang, J.; Yang, P. P.; Shen, Q. H.; Liu, J. Y.; Song, D. L.; Gao, Z.; Zhang, M. L. *J. Power Sources* **2013**, *235*, 45−53.
(32) Wang, H. L.; Gao, Q. M.; Jiang, L. *Small* **2011**, *7*, 2454−2459.
(33) Jiang, H.; Li, C. Z.; Sun, T.; Ma, J. *Chem. Commun.* **2012**, *48*, 2606−2608.
(34) He, Y. M.; Chen, W. J.; Li, X. D.; Zhang, Z. X.; Fu, J. C.; Zhao, C. H.; Xie, E. Q. *ACS Nano* **2013**, *7*, 174−182.
(35) Fan, Z. J.; Yan, J.; Wei, T.; Zhi, L. J.; Ning, G. Q.; Li, T. Y.; Wei, F. *Adv. Funct. Mater.* **2011**, *21*, 2366−2375.
(36) Yuan, C. Z.; Yang, L.; Hou, L. R.; Shen, L. F.; Zhang, X. G.; Lou, X. W. *Energy Environ. Sci.* **2012**, *5*, 7883−7887.
(37) Chen, S.; Xing, W.; Duan, J. J.; Hu, X. J.; Qiao, S. Z. *J. Mater. Chem. A* **2013**, *1*, 2941−2954.
(38) Yuan, C. Z.; Li, J. Y.; Hou, L. R.; Zhang, X. G.; Shen, L. F.; Lou, X. W. *Adv. Funct. Mater.* **2012**, *22*, 4592−4597.
(39) Zhang, G. Q.; Lou, X. W. *Sci. Rep.* **2013**, *3*, 1470−1475.